

The effect of low-energy ion-implantation on the electrical transport properties of Si-SiO₂ MOSFETs

D R McCamey^{1,2}, M Francis², J C McCallum^{1,3},
A R Hamilton^{1,2}, A D Greentree^{1,3} and R G Clark^{1,2}

¹ Australian Research Council Centre of Excellence for Quantum Computer Technology

² School of Physics, University of New South Wales, NSW 2052, Australia

³ School of Physics, University of Melbourne, VIC 3010, Australia

E-mail: dane.mccamey@unsw.edu.au

Abstract.

Using silicon MOSFETs with thin (5nm) thermally grown SiO₂ gate dielectrics, we characterize the density of electrically active traps at low-temperature after 16keV phosphorus ion-implantation through the oxide. We find that, after rapid thermal annealing at 1000°C for 5 seconds, each implanted P ion contributes an additional 0.08 ± 0.03 electrically active traps, whilst no increase in the number of traps is seen for comparable silicon implants. This result shows that the additional traps are ionized P donors, and not damage due to the implantation process. We also find, using the room temperature threshold voltage shift, that the electrical activation of donors at an implant density of $2 \times 10^{12} \text{cm}^{-2}$ is $\sim 100\%$.

PACS numbers: 73.40.-c , 73.40.Qv, 85.40.Ry

1. Introduction

Device fabrication involving ion implantation is widespread in the semiconductor industry, with applications ranging from ohmic contacts to shallow junctions [1, 2]. Methods to increase the performance of classical transformers [3], new types of classical computation [4], and a number of solid state implementations of quantum computation (QC) [5, 6, 7, 8, 9, 10], all involving ion-implantation of few or single ions, have been proposed. In the proposal by Hollenberg *et al* [9] for example, the position of the donor electron on one of two implanted [11] closely spaced P donors in Si act as the qubit.

In all of these devices, electrically active defects caused by ion implantation must be eliminated so that operations involving single electrons are not compromised. To ensure that this requirement is met, it is important to characterize the effects of ion implantation on the trap density. It is also important that all implanted donors be activated for the device to function correctly. Given that these devices are intended to be operated in the few or single electron regime, a non-activate donor anywhere in the device would strongly inhibit device function.

Previous studies of damage caused by ion implantation have mainly involved capacitive measurements (eg capacitance-voltage, Deep Level Transient Spectroscopy

[12]) or have focused on room temperature measurements [13]. This paper focuses on the characterization of implantation-induced defects in MOSFET devices using DC transport measurements at low-temperature, where silicon-based quantum computer devices are most likely to be operated. We also study the donor activation of these implants.

2. Method

MOSFETs are convenient to fabricate, have widely understood characteristics, and allow electrical measurements to be restricted to near the Si-SiO₂ interface [14], the area of interest for low-energy implantation studies. Additionally, the processing used in the fabrication of MOSFETs is expected to be compatible with the fabrication processes used, for example, in silicon-based quantum computer devices. This allows the possibility of fabricating on-chip characterization devices. For these reasons, MOSFETs were used to characterize the implant damage in this study.

2.1. Mobility and Critical Density at 4.2K

Numerous methods exist for characterizing the electrically active damage, or traps, at room temperature [15]. At cryogenic temperatures, where standard capacitance based methods fail due to the long thermal emission time, a number of more complex methods also exist [16]. Some simpler methods using the Hall effect involve comparing measured values of carrier density with theoretical predictions [17, 18]. We use a method that involves only conductance and Hall measurements, removing errors associated with comparison to theory and allowing for ease of measurement.

At low temperatures, the mobility, μ , of an electron in the inversion layer of a MOSFET as a function of the carrier density, n , is characterized by a critical density, n_{crit} , below which no conduction occurs. The lack of conductivity below the critical density is due to a freeze out of free carriers due to impurity binding [19]. The method used to characterize the trap density in this work is based on the above property. The mobility as a function of the carrier density was determined from Hall measurements. The critical density was then determined by extrapolating the linear region of μ vs $\log(n)$ above the critical density to zero. The trap density of the device is taken to be the critical density.

Measurements at 4.2K were performed to determine the number of electrically active traps present at these temperatures. The 4-terminal resistivity, ρ , of the inversion layer was measured at numerous gate voltages. Hall measurements were taken from B=0 to 0.5T, for at least 5 gate voltages per sample. The carrier density as a function of gate voltage was determined from these measurements. The mobility was determined using both the resistivity and the carrier density by the relation [1]

$$\mu = 1/(\rho ne). \quad (1)$$

2.2. Threshold Voltage Shift at Room Temperature

To determine the fraction of implanted ions that were activated, the threshold voltage shift was analyzed. Assuming the ions are implanted to a constant depth (ie a delta

function approximation), the relation between doping and threshold shift is given by [1]

$$n_{\text{act}} = \frac{\Delta V_{\text{th}} C_{\text{imp}}}{q} \quad (2)$$

where n_{act} is the number of activated donors per unit area, ΔV_{th} is the change in threshold voltage, and C_{imp} the capacitance per unit area between the implanted ion layer and the gate. As the implant distribution sits 20nm into the silicon, the capacitance is the sum of that due to the oxide and the silicon layer, ie

$$C_{\text{imp}} = [(1/C_{\text{ox}}) + (1/C_{\text{Si}})]^{-1} = [(d_{\text{ox}}/\epsilon_{\text{ox}}\epsilon_0) + (d_{\text{Si}}/\epsilon_{\text{Si}}\epsilon_0)]^{-1} \quad (3)$$

where d_{ox} is 5nm, ϵ_{ox} is 3.7, d_{Si} is 20nm and ϵ_{Si} is 11.9.

It is important to note that this method is only valid for ionised impurities, and for this reason the measurements were performed at room temperature. The effect of incomplete ionisation [20] is discussed with the results.

To confirm the validity of the delta approximation, once the number of ionised impurities was determined, the expected threshold shift was calculated using a model for the implants that consisted of a series of very thin, uniform implant regions that very closely followed the actual implant distribution. The threshold shift due to each of these was determined and the total shift found. There was a negligible (< 1%) difference between these methods, indicating that the original single delta approximation was sufficient.

Modelling, using a one-dimensional Poisson solver [21], of both implanted and unimplanted devices was also performed. The carrier density as a function of depth for a number of gate voltages was determined, and integrated to find the carrier density as a function of gate voltage. The threshold in these simulations was compared to the experimentally measured threshold, again confirming the density of activated ions.

2.3. Device Fabrication

The devices used in this study, Hall-bar geometry MOSFETs, were fabricated on a high resistivity (> 5000Ω.cm) n-type Si <100> substrate. After etching in a 10% HF solution for 10 seconds to remove the native oxide, a 5nm thermal oxide layer was grown. Two implant species, P and Si, were used, P as this is the most common donor in silicon and has important applications in QC proposals, and the Si as a control. A number of devices were then implanted with either P at 16keV or Si at 15keV. This results in an implant distribution centered approximately 20nm into the silicon, with a straggle of approximately 7nm [1]. A number of different doses were implanted, ranging from no implant to $5 \times 10^{12}\text{cm}^{-2}$. Rapid thermal annealing at 1000°C for 5 seconds in a N₂ ambient was then applied to all devices. For both the gate and ohmic metallization 200nm of Aluminium was used. Following metalisation, the devices were annealed at 400°C for 15 minutes in forming gas (5% Hydrogen, 95% Nitrogen).

3. Results

3.1. Implant Activation at Room Temperature

The I-V characteristics of the MOSFETs were measured at room temperature. The results for different P implant densities are shown in figure 1. The threshold voltage

The effect of ion-implantation on the electrical transport properties of Si-SiO₂ MOSFET's

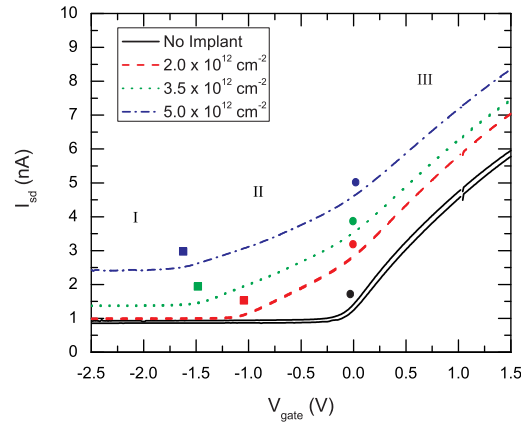


Figure 1. Source drain current as a function of Gate voltage, showing threshold voltage shift as a function of implant density. Measurements taken with a 100 μ V source drain voltage at room temperature. The squares indicate the threshold voltage after implantation. The circles show the location of the kink in the current at a similar voltage to the threshold in the unimplanted device. I, II, and III indicate three different conduction regimes, which are discussed in the text.

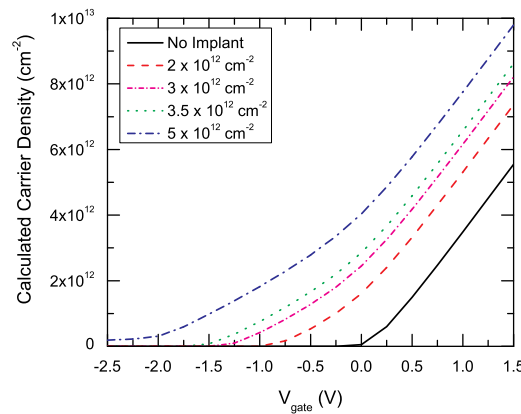


Figure 2. Calculated carrier density vs gate voltage, T=300K, implant range = 20nm, implant straggle = 7nm.

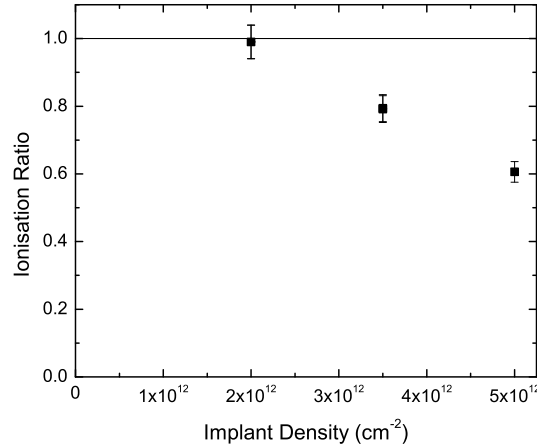


Figure 3. Measured ionisation ratio (number of activated ions times probability of ionisation divided by number of implanted ions) as a function of implant density for P implants at 16keV after rapid thermal annealing.

was taken to be the intersection of the linear fit to the sub-threshold current and the linear fit to the current in the region just above the point where the current deviates from the sub-threshold current. As expected, the threshold voltage is decreased by the addition of n-type dopants. The Si implanted control devices did not show a decrease in threshold voltage, which shows that the change in threshold is due to the incorporation of donors, and not the creation of charged damage during implantation.

The activation ratio is defined as the number of activated P atoms (ie those sitting in substitutional sites) divided by the number of implanted P ions. The threshold voltage shift is determined by the number of charged P donors, which is the product of the number of activated donors and the probability that they are ionised. Figure 3 shows the measured ionisation ratio (activation ratio times probability of activation) as a function of the implant dose. The ionisation ratio is found to decrease with increasing implant dose. This is expected, given that the fraction of ionised donors is known to decrease with increasing density of donors [23], due to the increased number of dopant states available, even at room temperature [20].

We note that recent studies of P-implanted silicon by spreading resistance analysis (SRA) have shown the opposite trend - that the apparent activation ratio increases with increasing implant dose [7, 22]. This discrepancy might possibly be explained by the presence of a native (poor quality) oxide with a high trap density in very close proximity to the implanted region, caused by cutting the wafer at a very shallow angle. If a significant density of electrons are caught in traps at the native oxide interface they do not contribute to conduction, so that the number of free electrons appears lower than that expected due to the implant dose. This effect would be particularly significant at low implant dose, where the native oxide trap density is much higher than the P density, but would be less important at high doses, leading to an apparent activation ratio that increases with increasing implant dose, as observed in [7, 22]. If this is the case, it means that spreading resistance measurements are not well suited to measurements of low dose, near surface implants - however, more

work on understanding the difference between these two measurement techniques is required.

It is significant however that after RTA and for an implant dose of $2 \times 10^{12} \text{cm}^{-2}$ with an average spacing of $\sim 7 \text{nm}$, the ionisation ratio is 0.99 ± 0.05 , indicating almost complete activation and ionisation. Assuming that this near complete activation holds for doses below $2 \times 10^{12} \text{cm}^{-2}$, this result suggests that it will be possible to fabricate a device where the donor spacing is $\sim 20 \text{nm}$, such as the qubit proposed by Kane [5], with almost complete donor activation.

Another interesting feature to note is the appearance of three distinct conduction regimes in the implanted devices, labeled I, II and III in figure 1. In region II, from threshold to the threshold associated with the unimplanted device, the device current increases near linearly. Above the unimplanted threshold, when the device enters inversion, the device current returns to the expected form but with an offset (region III). In region I, below threshold, there is a constant current unaffected by the gate voltage, but which increases with implant density. The source of this current is unknown. A possible explanation is that the silicon dioxide used as an implant mask was not thick enough, resulting in an implant in the area outside of the gated area. However, the thickness of the implant mask ($\sim 200 \text{nm}$) should be more than adequate to stop all of the implanted ions, which have a range of $\sim 15 \text{nm}$ in SiO_2 at 15keV [1]. Alternatively, Poisson modelling shows that there is a small increase in the carrier density deep in the silicon ($\sim 50 \text{nm}$) for implanted devices at negative gate voltages (see figure 4). This would explain the increased conduction, except that the carrier density at negative voltages is 5 orders of magnitude smaller than that at positive voltages, which does not explain the high current observed. More work is needed to understand the cause of this conduction.

Modelling of the devices using a one-dimensional Poisson solver [21] was undertaken, and the carrier density as a function of depth for a number of gate voltages are presented in figure 4. In the implanted devices, an increase in the carrier density, centered at the mean implant depth, d_{Si} , is observed. The density in this region increases with gate voltage, until the unimplanted threshold is reached. For higher gate voltages, the carrier density is dominated by the inversion layer adjacent to the Si-SiO₂ interface.

The total carrier density at a given gate voltage and implant density was determined by integrating the calculated carrier density to a depth of 100nm . The results are shown in figure 2. These traces have a similar form to the measured current (figure 1) showing the two distinct conduction regimes above threshold, but not the sub-threshold current. The effect of scattering can be seen in the deviation of the measured current from the calculated carrier density. The threshold however should not be effected by the scattering mechanisms, and the current should go to zero at the same gate voltage as the carrier density.

Calculations were performed for devices with P implants of 2, 2.7 and $3 \times 10^{12} \text{cm}^{-2}$, the density of activated donors determined from the threshold voltage shift. The threshold found in these calculations was in good agreement with that observed experimentally, and better than those simulations where the incomplete ionisation of donors was not considered. This indicates that the analysis of the activation ratio is correct.

To summarize, we find that there is a decrease in the threshold voltage due to the implantation of donors, although the magnitude of the decrease is smaller than expected. This may be due to the incomplete ionisation of the implanted donors,

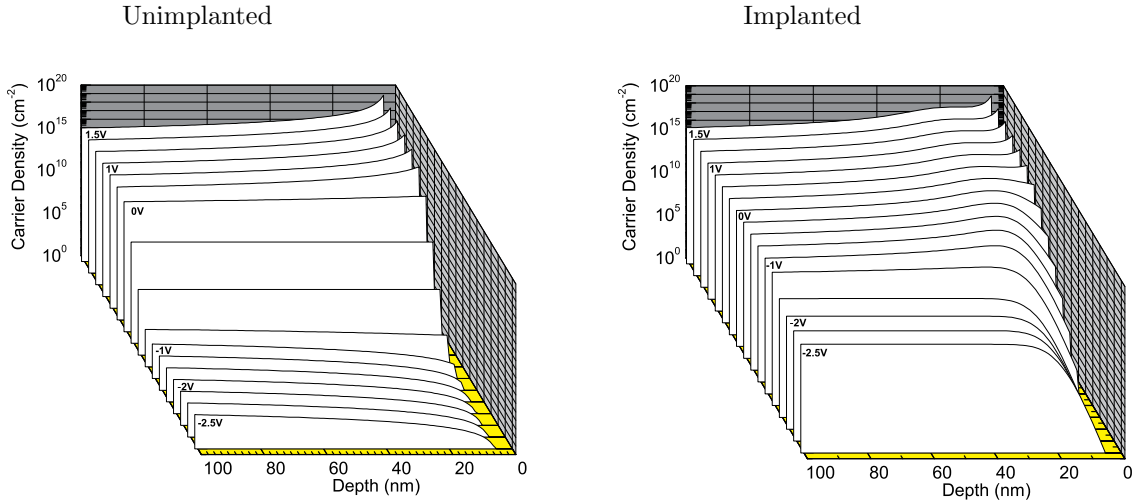


Figure 4. Calculated carrier density as a function of depth and Gate Voltage, at room temperature for an unimplanted MOSFET (left) and for a MOSFET with a P implant dose of $3.5 \times 10^{12} \text{ cm}^{-2}$ (right). $T = 300\text{K}$.

which serves to limit their effect on the threshold voltage. We find that for an implant of $2 \times 10^{12} \text{ cm}^{-2}$, the activation is near 100%.

3.2. Damage due to Implantation

We now turn to consider the damage caused by the implantation process. Figure 5 shows the mobility of P implanted MOSFET's, at a number of different doses. The traces show the usual form of the low temperature mobility, that is, at low density, an increasing mobility limited by impurity scattering, and at high density, a decreasing mobility limited by scattering due to interface roughness. Traces for a number of different implant densities are shown.

In the P implanted devices, the maximum mobility is seen to decrease and move to higher carrier densities (figure 6) as the implant dose is increased, indicating an increase in ionized impurity scattering. For Si implanted devices the mobility, shown in figure 5, does not show this effect. As the Si and P ions are of similar mass, and are implanted at similar energies, they should cause similar damage to the Si lattice during implantation. As the decrease in mobility is not seen in the Si implanted devices, the cause of the increased scattering does not appear to be the implantation process. This result suggests that the RTA is able to repair all damage from implantation. An alternate explanation is that stable P-related defects may form during the annealing process accounting for the increased trap density, but we believe that this will be a secondary effect when compared to the lattice damage caused during implantation.

It is important to note that there are variations in the mobilities across wafers and from chip to chip, however, the deviation between devices on a similar chip is much smaller than that from chip to chip from the same wafer, which is smaller again

The effect of ion-implantation on the electrical transport properties of Si-SiO₂ MOSFET's

than that from wafer to wafer. To combat this, the measurements for a given implant species were taken from single wafers. The wafers were cleaved into quarters, with each quarter implanted at a different dose, and one quarter being left unimplanted. As a result, it is difficult to compare numerically the results from wafer to wafer. This explains the higher peak mobility in the Si implanted devices compared to the P implanted devices.

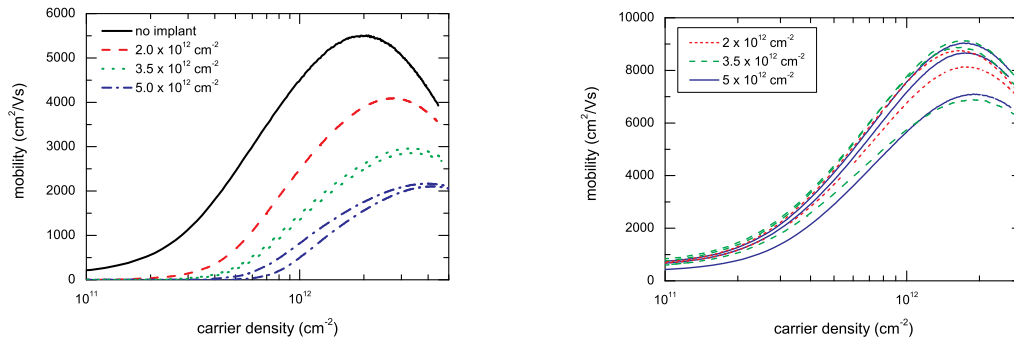


Figure 5. Mobility as a function of carrier density for MOSFET's with various P (left) and Si (right) implantation densities.

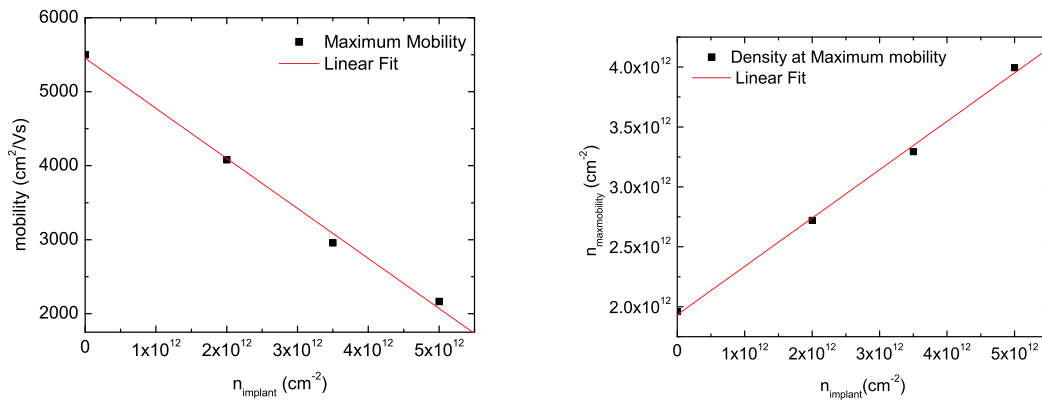


Figure 6. Maximum mobility (left) and carrier density at which maximum mobility occurs (right) as a function of P implant density. Both the decrease in mobility and the movement of peak mobility to higher density indicate an increase in charged impurity scattering as the implant dose is increased.

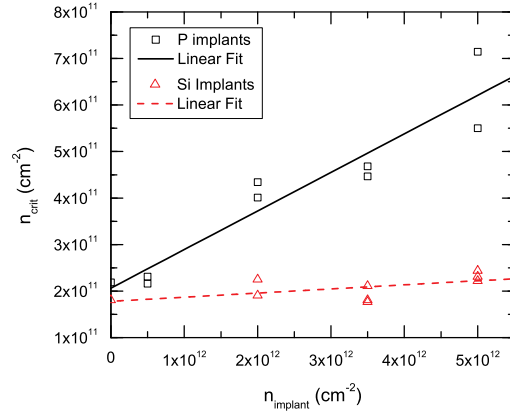


Figure 7. Trap density vs Implant density for both P and Si implanted devices. Linear fits to the data are shown. The data for P implants at $5 \times 10^{11} \text{cm}^{-2}$ is for a device fabricated on a separate wafer.

The critical density of both P and Si implanted devices is shown in figure 7. For P implanted devices, the critical density increases linearly with implant density. Equating the critical density with the trap density [19] shows that each implanted ion has an equivalent effect to the creation of 0.08 ± 0.03 additional traps. For Si implanted devices, this effect decreases to 0.009 ± 0.005 additional traps.

The above results can be explained by the straggle of the implanted ions. Modelling of the implanted ion distribution using data from [1] shows that, for the implant energy used, approximately 10% of implanted ions sit within 10nm of the interface. Modelling of the wavefunction using [21] and other studies [24] shows that electrons in the inversion layer are localized to within approximately 10nm of the Si-SiO₂ interface. Hence, only about 10% of the implanted ions will interact strongly with the electrons in the inversion layer.

Below threshold, there are no electrons in the 2DEG, and all donor electrons are bound to the P implants. Above threshold, when the channel is populated with electrons, the additional electrons serve to screen the P donors, and they are unable to localize any electron [24]. At this point, the ionized P donor serves to scatter the electrons in the 2DEG, leading to the increased ionized impurity scattering seen in figure 5. This also explains the movement of the critical density, as the electrons that are localized below the threshold are free to contribute to the Hall voltage, and thus the carrier density, above threshold.

The increase in the critical density (8% of implant) is in good agreement with the number of implanted donors near the 2DEG ($\sim 100\%$ of implant), again suggesting that RTA is able to remove all damage caused by implantation, and that the increased scattering and trapping is due only to the P donors close to the Si-SiO₂ interface.

Another important characteristic is the density of electron traps in the unimplanted device. This was found to be $2.1(\pm 0.3) \times 10^{11} \text{cm}^{-2}$. This equates to a trap spacing of $21.8 \pm 1.7 \text{ nm}$. For a Kane architecture quantum computer, this is approximately the qubit-qubit spacing (20nm). This means that for every implanted

P donor there is approximately one electron trap, which will interfere with device operation, either by localizing the donor electron or by other methods. While this density of traps may be suitable for fabrication of a small number of silicon-based qubits, it will need to be reduced, for example by improving the oxide quality, for the large scale (many qubit) implementations that are proposed.

4. Conclusions

We have characterized the density of electrically active traps at low temperature, using DC conductance measurements in silicon MOSFETs. We determine the effect of low-energy low-density Si and P ion implantation into a Si-SiO₂ system, and found that the Si implantation had no effect on the low temperature trap density, whilst the P implantation resulted in an additional 0.08(\pm 0.01) traps per implanted ion. We interpret these additional traps to be P donors in the conduction channel acting to localize donor electrons, and not damage due to implantation.

We also find that the electrical activation of the implanted donors to be near complete at a dose of $2 \times 10^{12} \text{cm}^{-2}$, falling to approximately 60% at a dose of $5 \times 10^{12} \text{cm}^{-2}$. This indicates that a device that requires a donor spacing of approximately 20nm, such as the Kane quantum computer, can be fabricated with near 100% activation using ion implantation.

Acknowledgments

The authors thank E. Gauja and S. Angus for assistance in device fabrication, R. P. Starrett and D. Barber for assistance with construction of low temperature measurement equipment and A. S. Dzurak for helpful discussions. This work was supported in part by the Australian Research Council, the Australian Government, the U.S. National Security Agency, the Advanced Research and Development Agency, and the U.S. Army Research Office under Contract No. DAAD19-01-1-0653.

References

- [1] Sze S M 1975 *Physics of Semiconductor Devices 2nd Edition* (New York: John Wiley & Sons)
- [2] Jones E C and Ishida E 1998 Shallow junction doping technologies for ULSI *Materials Science and Engineering: R: Reports* **R24** 1
- [3] Shinada T, Koyama H, Hinoshita C, Imamura K and Ohdomari I 2002 Improvement of focused ion-beam optics in single-ion implantation for higher aiming precision of one-by-one doping of impurity atoms into nano-scale semiconductor devices *Japanese Journal of Applied Physics Part 2 - Letters* **41** L287
- [4] Cole J H, Greentree A D, Wellard C J, Hollenberg L C L and Prawer S 2004 Quantum-Dot Cellular Automata using Buried Dopants *eprint arXiv:cond-mat/0407658*
- [5] Kane B E 1998 A silicon-based nuclear spin quantum computer *Nature* **393** 133
- [6] McKinnon R P, Stanley F E, Lumpkin N E, Gauja E, Macks L D, Mitic M, Chan V, Peceros K, Buehler T M, Dzurak A S, Clark R G, Yang C, Jamieson D N and Prawer S D 2002 Nanofabrication processes for single-ion implantation of silicon quantum computer devices *Smart Materials and Structures* **11** 735
- [7] Schenkel T, Persaud A, Park S J, Nilsson J, Bokor J, Liddle J A, Keller R, Schneider D H, Cheng D W and Humphries D E 2003 Solid state quantum computer development in silicon with single ion implantation *Journal of Applied Physics* **94** 7017
- [8] Vrijen R, Yablonovitch E, Wang K, Jiang H W, Balandin A, Roychowdhury V, Mor T and DiVincenzo D 2000 Electron-spin-resonance transistors for quantum computing in silicon-germanium heterostructures *Physical Review A* **62** 012306

- [9] Hollenberg L C L, Dzurak A S, Wellard C, Hamilton A R, Reilly D J, Milburn G J and Clark R G 2004 Charge-based quantum computing using single donors in semiconductors *Physical Review B* **69** 113301
- [10] Clark R G, Brenner R, Buehler T M, Chan V, Curson N J, Dzurak A S, Gauja E, Goan H S, Greentree A D, Hallam T, Hamilton A R, Hollenberg L C L, Jamieson D N, McCallum J C, Milburn G J, O'Brien J L, Oberbeck L, Pakes C I, Prawer S D, Reilly D J, Ruess F J, Schofield S R, Simmons M Y, Stanley F E, Starrett R P, Wellard C and Yang C 2003 Progress in silicon-based quantum computing *Philosophical Transactions of the Royal Society of London Series A - Mathematical Physical and Engineering Sciences* **361** 1451
- [11] Dzurak A S, Hollenberg L C L, Jamieson D N, Stanley F E, Yang C, Bühler T M, Chan V, Reilly D J, Wellard C, Hamilton A R, Pakes C I, Ferguson A G, Gauja E, Prawer S, Milburn G J and Clark R G 2003 Charge-based silicon quantum computer architectures using controlled single-ion implantation *eprint arXiv:cond-mat/0306265*
- [12] Yamasaki K, Yoshida M, Sugano T 1979 Deep level transient spectroscopy of bulk traps and interface states in Si MOS diodes *Japanese Journal of Applied Physics* **18** 113
- [13] Peterström S 1993 Si-SiO₂ interface trap density in boron and phosphorus-implanted silicon *Applied Physics Letters* **63** 672
- [14] Sun S C and Plummer J D 1980 Electron mobility in inversion and accumulation layers on thermally oxidized silicon surfaces *IEEE Transactions on Electron Devices* **27** 1497
- [15] Witczak S C, Suehle J S and Gaitan M 1992 An experimental comparison of measurement techniques to extract Si-SiO₂ interface trap density *Solid-State Electronics* **35** 345
- [16] Divakaruni R and Viswanathan C R 1995 Quasi-static behaviour of MOS devices in the freeze-out regime 1995 *IEEE Transactions on Electron Devices* **42** 87
- [17] Saks N S, Ancona M G and Rendell R W 2002 Using the Hall effect to measure interface trap densities in silicon carbide and silicon metal-oxide-semiconductor devices. *Applied Physics Letters* **80** 3219
- [18] Fang F F and Fowler A B 1968 Transport Properties of Electrons in Inverted Silicon Surfaces. *Physical Review* **169** 619
- [19] Das Sarma S and Hwang E H 1999 Charged impurity-scattering-limited low-temperature resistivity of low-density silicon inversion layers *Physical Review Letters* **83** 164
- [20] Xiao G, Lee J, Liou J J and Ortiz-Conde A 1999 Incomplete ionization in a semiconductor and its implications to device modelling *Microelectronics Reliability* **39** 1299
- [21] Snider G 1996 1D Poisson/Schrodinger Solver <http://www.nd.edu/~gsnider/>
- [22] Park S -J, Persaud A, Liddle J A, Nilsson J, Bokor J, Schneider D H, Rangelow I W, Schenkel T 2004 Processing issues in topdown approaches to quantum computer development in silicon *Microelectronic Engineering* **73-74** 695
- [23] Singh J 2001 *Semiconductor Devices: Basic Principles* (New York: John Wiley & Sons). In equation 2.34 on page 80 we see that $\frac{n_d}{n+n_d} = \frac{1}{\frac{N_c}{2N_d} \exp\left[-\frac{(E_c-E_d)}{k_B T}\right] + 1}$.
- [24] Stern F and Howard W E 1967 Properties of semiconductor surface inversion layers in the electric quantum limit *Physical Review* **163** 816